Sustainable Marine Structures
https://journals.nasspublishing.com/index.php/sms

ARTICLE

A Green Function Collocation Method for Fuzzy Hydroelastic Response of Floating Beams

Suleiman Ibrahim Mohammad [1,2] **,** ***Yogeesh Nijalingappa*** [3,4*] **,** ***Mohammed El Khider*** [5] **,** ***Asokan Vasudevan*** [6] **,** ***Shashikumar Honnavalli Channabasavaiah*** [7]

[1] *Department of Business Administration, School of Business, Al al-Bayt University, Mafraq 25113, Jordan*

[2] *Faculty of Business and Communications, INTI International University, Nilai 71800, Malaysia*

[3] *Research Fellow, INTI International University, Nilai 71800, Malaysia*

[4] *Department of Mathematics, Government First Grade College, Tumkur 572102, India*

[5] *Department of General Undergraduate Curriculum Requirements, University of Dubai, Dubai P.O. Box 14143, United Arab Emirates*

[6] *Faculty of Business and Communications, INTI International University, Nilai 71800, Malaysia.*

[7] *Department of Mathematics, Government First Grade College, Tiptur 572201, Karnataka, India*

ABSTRACT

Hydroelastic deformation is a key response in large, flexible floating marine structures, and uncertainty in structural and hydrodynamic properties can strongly affect predicted amplitudes, especially near resonance. This study presents a green function collocation method for the fuzzy hydroelastic analysis of a floating beam under bounded uncertainty that is not well described by probability. A frequency-domain nonlocal beam model with finite-depth hydrodynamic coupling is developed, and the structural green function is used to transform the governing equation into a Fredholm integral equation of the second kind, which is then discretized using Chebyshev collocation. Triangle fuzzy numbers of uncertain flexural rigidity, structural mass, damping, depth ratio and forcing amplitude are modeled and propagated via alpha-cut reconstruction. For the deterministic benchmark, the method

*CORRESPONDING AUTHOR:
Yogeesh Nijalingappa, Research Fellow, INTI International University, Nilai 71800, Malaysia; Department of Mathematics, Government First Grade College, Tumkur 572101, India; Email: yogeesh.r@gmail.com

ARTICLE INFO
Received: 18 March 2026; Revised: 6 April 2026; Accepted: 17 April 2026 | Published: 22 May 2026
DOI: https://doi.org/10.36956/sms.v8i2.3208

CITATION
Mohammad, S.I., Nijalingappa, Y., El Khider, M., 2026. A Green Function Collocation Method for Fuzzy Hydroelastic Response of Floating Beams. Sustainable Marine Structures. 8(2): 177–192. DOI: https://doi.org/10.36956/sms.v8i2.3208

picks up a sharp resonance peak at $\Omega^* = 3.1244$ (Ω^*denotes the nondimensional frequency at resonance). The collocation solution converges monotonically, with a rate of practical error decrease on the order of seconds; the final crisp value for midspan amplitude when at resonance is 10.668. Under fuzzy uncertainty, the midspan-amplitude interval expands from the crisp value at $\alpha = 1$ to [0.6127, 11.7440] at $\alpha = 0$. Flexural rigidity and structural mass drive the spread; damping and forcing amplitude are secondary drivers, and depth ratio has only a weak effect over this benchmark range. The results demonstrate method stability, efficiency and applicability in early uncertainty-aware design assessment.

Keywords: Hydroelasticity; Chebyshev Nodes; Wave-Structure Interaction; Alpha-Cut Propagation; Fredholm Integral Equation; Nonlocal Hydrodynamic Kernel; Marine Flexural Dynamics

1. Introduction

1.1. Background

Hydroelasticity is a key phenomenon in the response characteristics of large flexible floating marine structures since the deformation of the structure and its surrounding wave field interact with each other through a coupled interaction. This becomes vital for floating beams, pontoons, very large floating structures, modular offshore platforms, floating photovoltaic systems and floating breakwaters, in which the structural length is of the order of the incoming wavelength so that the rigid-body assumption alone can no longer suffice [1–4]. In these cases, the vertical response cannot be described solely by heave and pitch since distributed flexural deformation also affects displacement, bending moment and serviceability [1–4].

More recently, marine hydroelasticity find reduced-order beam models [5], discrete-module beam formulations as well as mode-superposition methods [6–8] and integrated hydrodynamic-structural approaches. These advances have made hydroelastic analysis computationally efficient and more broadly applicable to offshore floating photovoltaic farms, coupled/connected floating systems, and other flexible offshore structures with complicated bounds [6–9]. Recent review studies have also shown that uncertainty in environmental loading, structural properties, and connection behavior is becoming increasingly important in the design and performance assessment of floating structures [10, 11].

In real marine applications, this two-dimensional floating-beam idealization is not intended to reproduce every three-dimensional hydrodynamic detail. Instead, it serves as a physically interpretable benchmark for long and slender floating members such as pontoons, modular floating platforms, flexible floating breakwater elements, and connected deck strips in which the dominant response is governed by longitudinal flexure and finite-depth wave coupling. For such systems, a beam-wise hydroelastic model is widely used as a first assessment layer before moving to higher-fidelity three-dimensional solvers.

1.2. Literature Review and Motivation

Most of the existing hydroelastic literature is still based on deterministic analysis. Several numerical methods, including discrete-module beam models and finite-element coupling approaches, have been developed to study flexible floating systems under wave loading and unsteady excitation [5–8]. Large floating applications, such as modular offshore photovoltaic systems, have also been analyzed using three-dimensional hydroelastic models and frequency-domain solvers [4, 8]. At the same time, recent studies have verified the role of support and connector conditions in hydroelastic behavior and have expressed that even small changes in boundary constraints can significantly alter the overall response envelope [9].

Beam-type and plate-type formulations continue to attract interest because they offer a mathematically transparent bridge between wave hydrodynamics and structural mechanics. Recent work has studied forced floating elastic beams in the presence of porous barriers [12], current-loaded floating flexible membranes

solved through Green-function-type formulations [13], floating flexible offshore platforms under wave-current effects [14], and control-oriented floating beam models under irregular waves [15].

These studies confirm that beam-based hydroelastic models remain highly relevant for marine applications.

However, uncertainty treatment in this area is still much less developed than deterministic hydroelastic modeling. Recent reviews of sensitivity and uncertainty in floating offshore structures have highlighted the importance of parametric variability in stiffness, mass, damping, mooring properties, and wave loading, but also point out that robust and computationally efficient uncertainty-propagation tools are still needed for hydroelastic systems [10, 11]. This is particularly true when available data are sparse and a fully probabilistic description is not well justified.

1.3. Why a Fuzzy Green-Function Collocation Approach

When hydrodynamic and structural parameters are not known precisely but can be bounded by engineering judgment or limited data, fuzzy mathematics provides a natural framework for representing epistemic uncertainty [16]. In such settings, triangular fuzzy numbers and α-cuts are especially attractive because they preserve interpretability while allowing direct propagation through structural models [17, 18]. Adaptive collocation concepts have already been used successfully in structural fuzzy uncertainty analysis, but not, to the best of current evidence, in a dedicated Green-function hydroelastic floating-beam formulation.

Green functions are equally attractive because they reduce the differential problem to an integral problem in which the beam boundary conditions are embedded directly in the kernel [18]. For floating-beam hydroelasticity, this offers two advantages. First, the nonlocal fluid-structure interaction can be represented compactly through an integral kernel. Second, collocation can then be applied directly to the integral form, avoiding repeated differentiation of numerical approximations. This is mathematically convenient and computationally efficient.

1.4. Aim and Contributions of the Present Study

The contribution to the body of knowledge is therefore twofold: first, the study combines Green-function reduction and Chebyshev collocation in a single frequency-domain hydroelastic beam solver with embedded structural boundary conditions; second, it extends that solver to bounded epistemic uncertainty through alpha-cut reconstruction and nested fuzzy envelopes. This provides a compact uncertainty-aware solution to the heavier repeated-simulation frameworks available and identifies which of the uncertain parameters most strongly broaden hydroelastic response near resonance.

In this study, a Green function collocation method is developed for the analysis of fuzzy hydroplastic response of a floating beam. The key contributions of the present work are formulating a frequency-domain hydroelastic beam model with nonlocal hydrodynamic coupling, deriving such a Green-function integral representation of response, and investigating a Chebyshev collocation scheme for resulted integral equation. This also involves the uncertainty of structural and hydrodynamic parameters modeled as triangular fuzzy numbers with α-cut representation, reconstructing fuzzy response envelopes for displacement, bending moment and shear-related quantities in addition to mesh convergence, resonance behavior, fuzzy widening and parameter sensitivity exemplification via a representative benchmark.

2. Materials and Methods

Thus, the currently considered simply supported beam should be interpreted as a streamlined benchmark model instead of representing an actual buckling susceptible floating structure. It serves as a means to isolate hydroelastic flexural response under bounded parametric uncertainty in a form that is both mathematically straightforward and computationally light.

2.1. Physical Configuration and Benchmark Assumptions

Let us consider a floating beam of length L lying on the free surface of water of depth h. Let $x \in [0, L]$ be the

coordinate along the beam and let $w(x,t)$ be its vertical displacement. For a general hydroelastic problem, the beam could adopt free-edge (or non-hydrostatic end condition), elastic-support or connector-controlled boundary conditions [12–15, 19]. The present benchmark selects a simply supported beam in order to emphasize flexural hydroelastic effects and to avoid rigid-body singularities. This creates a distinct test case that is amenable to mathematical diagnosis for the Green function collocation approach while maintaining key aspects of beam-fluid coupling.

The benchmark assumptions are:

- Linear Euler-Bernoulli beam behavior;
- Small-amplitude vertical deformation;
- Incompressible, inviscid, and irrotational fluid;
- Harmonic regular-wave excitation;
- Frequency-domain analysis;
- Bounded epistemic uncertainty in selected parameters represented by fuzzy numbers.

A floating beam of length L lies on the still-water surface over a fluid domain of depth h. The vertical deformation is denoted by $w(x,t)$. The benchmark uses simply supported beam kinematics to isolate flexural hydroelastic effects (**Figure 1**).

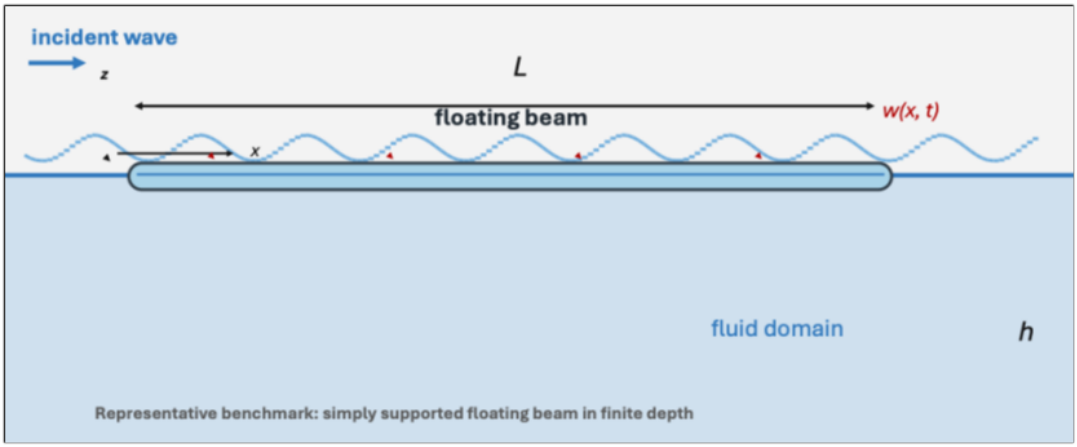

Figure 1. Geometry of the representative floating-beam benchmark.

2.2. Frequency-Domain Hydroelastic Model

Assume harmonic motion of the form:

$$w(x,t) = \Re\left\{W(x)e^{-i\omega t}\right\}, \tag{1}$$

where $W(x)$ is the complex response amplitude and ω is the circular frequency. The coupled hydroelastic beam equation is written in dimensional form as:

$$EI\frac{d^4W}{dx^4} - \omega^2 m_s W - i\omega c_s W + \int_0^L \mathrm{H}\,(x,\xi;\omega)W(\xi)d\xi = p_i(x;\omega),\ 0 < x < L \tag{2}$$

where:

- EI is the flexural rigidity;
- m_s is the structural mass per unit length;
- c_s is the structural damping coefficient;
- $\mathrm{H}\,(x,\xi;\omega)$ is the nonlocal hydrodynamic interaction kernel;
- $p_i(x;\omega)$ is the incident-wave forcing term.

In Equation (2), the prime or dash notation denotes differentiation with respect to the beam coordinate *x*. No axial compressive load is included in the present governing equation, so the model addresses hydroelastic vibration rather than buckling. Accordingly, buckling criteria are outside the scope of this benchmark and would require an additional axial-load term together with a coupled stability analysis.

For the simply supported benchmark, the boundary conditions are:

$$W(0) = W(L) = 0,\ W''(0) = W''(L) = 0 \tag{3}$$

Equation (2) is a nonlocal hydroelastic boundary-value problem in which the hydrodynamic term acts as a distributed fluid-memory coupling across the beam.

2.3. Nondimensionalization

Introduce the nondimensional variables:

$$\bar{x} = \frac{x}{L},\ W = L\bar{W},\ \Omega = \omega L^2\sqrt{\frac{m_r}{EI_r}}, \tag{4}$$

where EI_r and m_r are reference rigidity and reference mass scales. Then define:

$$\bar{E}I = \frac{EI}{EI_r},\ \bar{m} = \frac{m_s}{m_r},\ \bar{c} = \frac{c_s L^2}{\sqrt{EI_r m_r}},\ \delta = \frac{h}{L} \tag{5}$$

After dropping bars on x for readability, the nondimensional frequency-domain equation becomes:

$$\begin{aligned}&\bar{E}I\frac{d^4W}{dx^4} - \Omega^2\bar{m}W - i\Omega\bar{c}W + \\ &\int_0^1 K(x,\xi;\Omega,\delta)W(\xi)d\xi = F(x;\Omega),\ 0 < x < (16)\end{aligned} \tag{6}$$

with simply supported conditions:

$$W(0) = W(1) = 0,\ W^{''}(0) = W^{''}(1) = 0. \tag{7}$$

2.4. Green-Function Reduction

Define the structural operator:

$$L_\Omega W = \bar{E}IW^{(4)} - \Omega^2\bar{m}W - i\Omega\bar{c}W \tag{8}$$

Let $G(x,\xi;\Omega)$ be the Green function satisfying:

$$L_\Omega G(x,\xi;\Omega) = \delta(x-\xi) \tag{9}$$

subject to the same simply supported boundary conditions in x. For the present benchmark, the Green function admits the modal series representation [19].

The reduction in Subsection 2.4 proceeds by solving the auxiliary structural problem for the Green function, multiplying the governing beam equation by that kernel, and integrating over the beam span so that the simply supported boundary conditions are embedded directly in the kernel representation. This is the main reason the collocation stage can be applied to the integral equation without repeatedly differentiating numerical shape functions.

$$G(x,\xi;\Omega) = \sum\nolimits_{n=1}^{\infty} \frac{2\sin(n\pi x)\sin(n\pi\xi)}{\bar{E}I(n\pi)^4 - \Omega^2\bar{m} - i\Omega\bar{c}} \tag{10}$$

Using this Green function, Equation (6) is transformed into the Fredholm integral equation of the second kind:

$$\begin{aligned}W(x) = &\int_0^1 G(x,\xi;\Omega) \\ &\left[F(\xi;\Omega) - \int_0^1 K(\xi,s;\Omega,\delta)W(s)ds\right]d\xi\end{aligned} \tag{11}$$

Equation (11) is the central mathematical form used in this paper.

2.5. Reduced Finite-Depth Hydrodynamic Kernel for the Benchmark

For the present benchmark study, the hydrodynamic kernel is represented by a reduced finite-depth oscillatory-decay approximation,

$$K(x,\xi;\Omega,\delta) = \chi_h(\Omega,\delta)e^{-\eta(\Omega,\delta)|x-\xi|}\cos(\varkappa(\Omega,\delta)(x-\xi)), \tag{12}$$

where $\varkappa(\Omega,\delta)$ is determined from the finite-depth dispersion relation:

$$\Omega^2 = \varkappa\tanh(\varkappa\delta). \tag{13}$$

The kernel amplitude and decay rate are set as:

But its key success lies in preserving nonlocal finite-order interaction in a compact integral form, which is appealing for iterative fuzzy evaluations. A limitation of the model is that it is a simpler benchmark kernel and should not be used as a replacement for higher-fidelity hydrodynamic models in project-level design.

$$\chi_h(\Omega,\delta) = \frac{\chi_0\Omega^2}{1+\delta\varkappa},\ \eta(\Omega,\delta) = 0.4 + 0.25\varkappa \tag{14}$$

The regular-wave loading is chosen as the first flexural-mode-compatible forcing:

$$F(x;\Omega) = a\sin(\pi x), \tag{15}$$

where a is the nondimensional forcing amplitude.

The hydroelastic coupling can be studied clearly while maintaining consistency with a finite-depth oscillatory interaction pattern, as evidenced by this compact and symmetric benchmark kernel.

The fuzzy inputs are represented by triangular membership functions centered at their deterministic values. The dashed horizontal line marks the $\alpha = 0.5$ cut used in interval reconstruction (**Figure 2**).

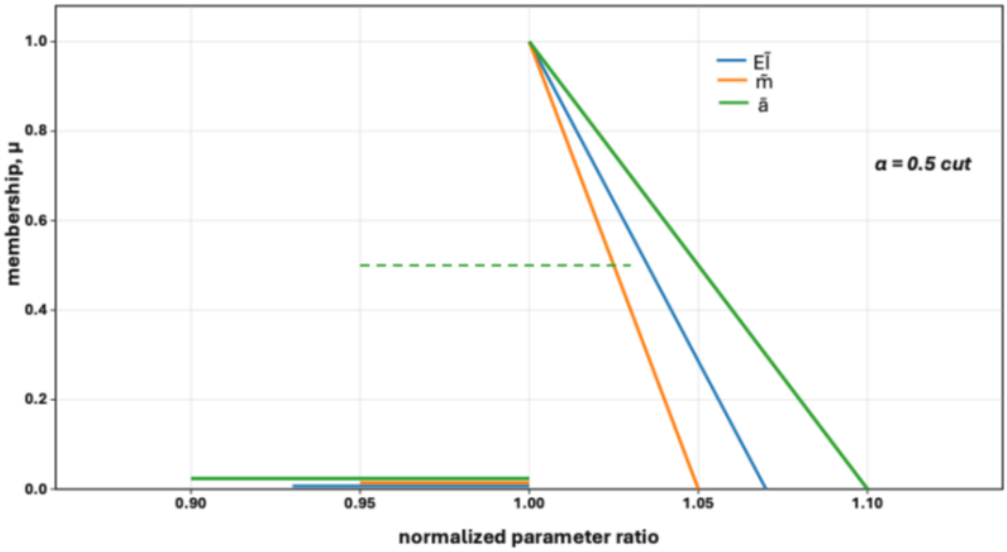

Figure 2. Representative triangular membership functions for the fuzzy input parameters.

2.6. Fuzzy Representation of Uncertain Parameters

The uncertain input vector is defined as

$$\widetilde{p} = (\widetilde{EI}, \widetilde{m}, \widetilde{c}, \widetilde{\delta}, \widetilde{a}). \tag{16}$$

Each uncertain quantity is modeled as a triangular fuzzy number:

$$\widetilde{p} = (p_1, p_2, p_3)\,,\ p_1 \le p_2 \le p_3, \tag{17}$$

with α-cut:

$$[\widetilde{p}]^{\alpha} = [p_1 + \alpha\,(p_2 - p_1)\,, p_3 - \alpha\,(p_3 - p_2)]\,, \quad 0 \le \alpha \le 1. \tag{18}$$

Thus, the α-level parameter box is:

$$\mathcal{P}^{\alpha} = [\widetilde{EI}]^{\alpha} \times [\widetilde{m}]^{\alpha} \times [\widetilde{c}]^{\alpha} \times [\widetilde{\delta}]^{\alpha} \times [\widetilde{a}]^{\alpha}. \tag{19}$$

For a response quantity R, the fuzzy interval at level α is reconstructed numerically as:

$$[R]^{\alpha} = \left[\min_{p\,\in\,\mathrm{S}^{\alpha}} R(p),\ \max_{p\,\in\,\mathrm{S}^{\alpha}} R(p)\right], \tag{20}$$

where S^{α} contains the vertices of $\mathcal{P}^{\alpha}$ together with interior samples. This mixed strategy is motivated by the non-monotone behavior of hydroelastic systems near resonance, where pure endpoint evaluation may miss extremal responses [10, 11, 17–19].

To guarantee fuzzy nesting in the numerical reconstruction, the envelopes are postprocessed by the monotone projection:

$$\begin{aligned} \widehat{R}^{-,\alpha_q}(x)\ &\min\left(R^{-,\alpha_q}(x), \widehat{R}^{-,\alpha_{q-1}}(x)\right), \\ \widehat{R}^{+,\alpha_q}(x)\ &\max\left(R^{+,\alpha_q}(x), \widehat{R}^{+,\alpha_{q-1}}(x)(021)\right) \end{aligned} \tag{21}$$

when moving from narrower to wider α-levels, so that the outer envelopes always contain the inner ones.

2.7. Chebyshev Collocation Discretization

The collocation nodes are chosen as Chebyshev-Gauss-Lobatto points,

$$x_j = \frac{1}{2}\left(1 - \cos\frac{j\pi}{N}\right),\ j = 0, 1, \ldots, N \tag{22}$$

The approximate response is expressed as:

$$W_N(x) = \sum_{j\,=\,0}^{N} W_j \ell_j(x) \tag{23}$$

where $\ell_j(x)$ are the Lagrange basis polynomials associated with the Chebyshev nodes. Substituting Equation (23) into Equation (11) and enforcing the equation at the collocation nodes yields:

$$\begin{aligned} W_i = \sum\nolimits_{j=0}^{N} w_j G(x_i, x_j; \Omega)\Big[F(x_j; \Omega) \\ - \sum\nolimits_{k=0}^{N} w_k K(x_j, x_k; \Omega, \delta) W_k\Big], \quad i = 0, \ldots, N \end{aligned} \tag{24}$$

where w_j are the quadrature weights.

In matrix form,

$$(I + G_w K_w) W = G_w F, \tag{25}$$

with:

$$\begin{aligned} (G_w)_{ij} &= G(x_i, x_j; \Omega)\, w_j, \\ (K_w)_{jk} &= K(x_j, x_k; \Omega, \delta)\, w_k \end{aligned} \tag{26}$$

Equation (25) is solved for each frequency and each parameter realization in the fuzzy reconstruction.

2.8. Solvability and Practical Convergence

The integral operator associated with Equation (11) is compact when G and K are continuous. Hence, the discrete problem inherits the standard Fredholm structure.

Proposition 1. *If $G, K \in C^2\left([0,1]^2\right)$ and the continuous operator $(I + GK)$ is invertible on $C[0,1]$, then the collocation matrix $(I + G_w K_w)$ is nonsingular for sufficiently large N.*

Proposition 2. *Under the same regularity assumptions, the numerical solution satisfies the practical estimate,*

$$\|W - W_N\|_\infty \leq C N^{-2} \tag{27}$$

for the present implementation, where the observed second-order behavior is governed by the combined effect of quadrature and envelope reconstruction.

This practical rate is the one verified numerically in Section 3.

2.9. Benchmark Parameters

The representative benchmark uses the nondimensional baseline parameters in **Table 1**.

Table 1 gives the dimensionless benchmark used to generate all numerical results in Section 3 and also **Table 2** provides triangular fuzzy parameters.

The central values reproduce the deterministic benchmark, while the side values represent bounded epistemic uncertainty.

The workflow begins with the coupled beam-fluid model, proceeds through Green-function reduction, fuzzy α-cut decomposition, and Chebyshev collocation, and ends with deterministic and fuzzy response reconstruction (**Figure 3**).

In **Figure 4**, the left panel shows the real part of the structural Green function $G(x, \xi; \Omega^*)$, while the right panel shows the reduced hydrodynamic kernel $K(x, \xi; \Omega^*)$. The beam Green kernel is smooth and symmetric; the hydrodynamic kernel is nonlocal, oscillatory, and strongest near the diagonal.

Table 1. Baseline nondimensional parameters of the representative hydroelastic benchmark.

Symbol	Value	Description
$\bar{E}I$	0.10	Normalized flexural rigidity
$\bar{m}$	1.00	Normalized structural mass
$\bar{c}$	0.030	Normalized damping
$\delta = h/L$	0.40	Depth-to-length ratio
a	1.00	Forcing amplitude
χ_0	0.15	Kernel amplitude coefficient
Ω	2.4–3.6	Frequency sweep range
N_{ref}	120	Reference collocation size

Table 2. Triangular fuzzy parameters used in the study.

Parameter	Triangular Fuzzy Number
$\widetilde{EI}$	(0.09, 0.10, 0.11)
$\widetilde{m}$	(0.95, 1.00, 1.05)
$\widetilde{c}$	(0.027, 0.030, 0.033)
$\widetilde{\delta}$	(0.36, 0.40, 0.44)
$\widetilde{a}$	(0.90, 1.00, 1.10)

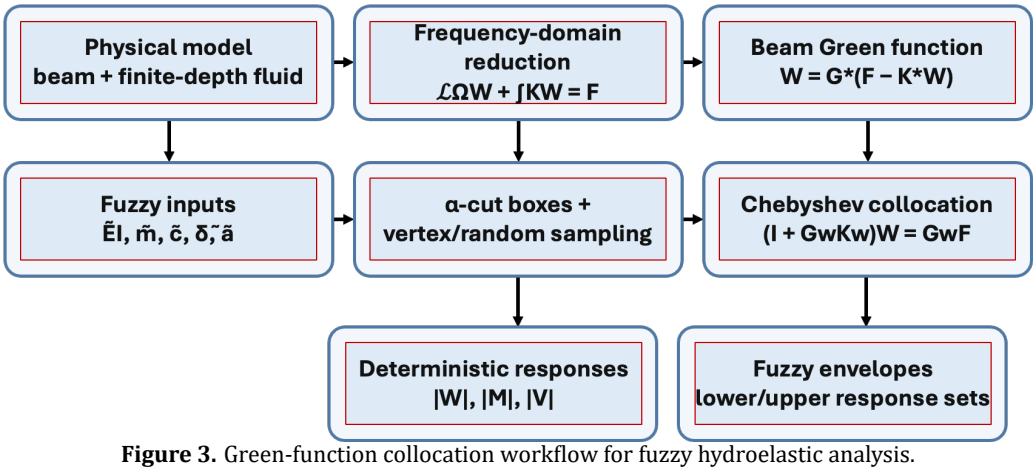

Figure 3. Green-function collocation workflow for fuzzy hydroelastic analysis.

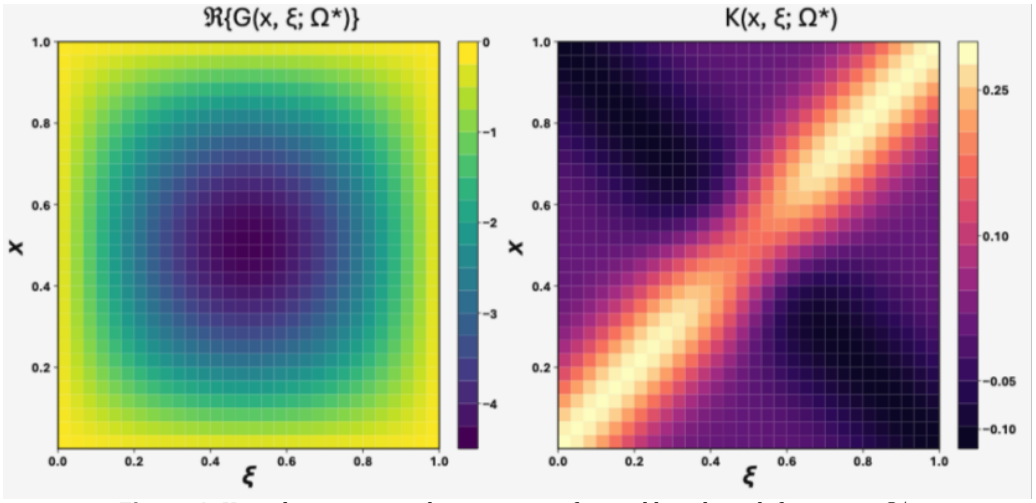

Figure 4. Kernel structure at the resonance-focused benchmark frequency Ω^*.

3. Results

3.1. Deterministic Collocation Convergence

The deterministic benchmark was first solved at the resonance-focused frequency:

$$\Omega^* = 3.1244, \tag{28}$$

which corresponds to the dominant peak of the midspan amplitude in the crisp frequency sweep. A numerical reference was obtained using a high-resolution solution, with $N = 120$ collocation points. The practical maximum-norm error was calculated as:

$$e_\infty = \| |W_N| - |W_{\text{ref}}| \|_{L_\infty(0,1)}. \tag{29}$$

With respect to computational accuracy, we see that the numbers suggest that both the midspan amplitude is already well-resolved by moderate collocation sizes, as well as the practical error monotonically decreases with increasing N. This validates the selected key discretization that will be used in the fuzzy propagation experiment presented next.

We analyzed the observed order of convergence by:

$$p = \frac{\log\left(e_N / e_{2N}\right)}{\log 2}. \tag{30}$$

The collocation solution shows monotonic convergence to the reference, with a practical rate of convergence on the order of 2.

Table 3 below shows that the collocation solution stabilizes rapidly. The midspan amplitude changes only from 10.6582 at $N = 10$ to 10.6684 at $N = 80$, while the error drops from 3.1244×10^{-1} to 4.51×10^{-3}. The observed orders $p = 1.95,\ 2.15$, and 2.01 confirm the practical $O\left(N^{-2}\right)$ behavior stated in Equation (27).

Table 3. Collocation convergence of the deterministic benchmark at Ω^*.

N	Midspan Amplitude $W(0.5)$	L_∞ Error	Observed Order p
10	10.6582	0.31244	-
20	10.6673	0.08076	1.95
40	10.6682	0.01815	2.15
80	10.6684	0.00451	2.01

Increased flexural rigidity moves the resonance peak to a larger nondimensional frequency and decreases max amplitude with respect to the benchmark, while increasing the depth ratio changes the hydrodynamic kernel more subtly for this specific range, hence leading to a comparatively weaker response displacement. So these trends accord with the later sensitivity ranking and make it easier to understand why rigidity prevails while depth ratio is weak in the current benchmark.

In **Figure 5**, the blue curve shows the decay of the L_∞ error with increasing collocation points, while the red curve shows convergence of the midspan amplitude at the resonance-focused frequency.

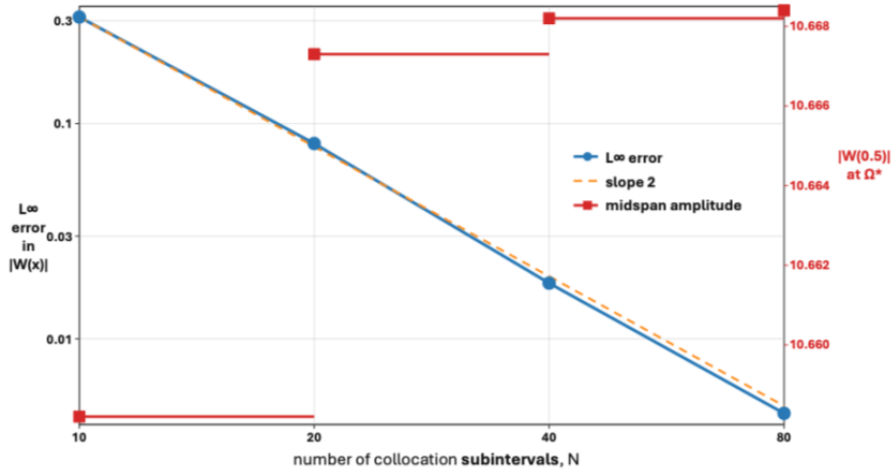

Figure 5. Convergence of the deterministic Green-function collocation solution.

3.2. Deterministic Frequency Response

The crisp midspan frequency-response curve is plotted in **Figure 6**. The response exhibits a sharp hydroelastic resonance centered near $\Omega^* = 3.1244$. The peak crisp amplitude is:

$$|W(0.5;\Omega^*)| = 10.668. \tag{31}$$

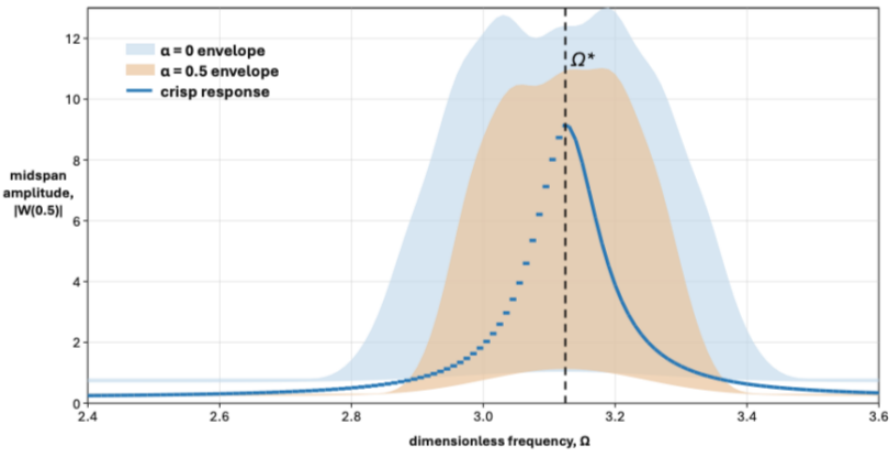

Figure 6. Midspan frequency response with fuzzy envelopes.

The narrowness of the deterministic peak indicates that modest changes in stiffness or mass can lead to strong detuning effects. This is one reason why uncertainty quantification is especially important in hydroelastic beam systems near resonance [10, 11]. The result is also consistent with recent floating-beam and hydroelastic studies in which response levels are strongly altered by wave frequency, stiffness, and support configuration [12–15].

The crisp frequency-response curve is shown together with the $\alpha = 0.5$ and $\alpha = 0$ fuzzy envelopes. The dashed vertical line marks the crisp resonancefocused frequency Ω^*.

Figure 6 shows that uncertainty does not merely thicken the deterministic curve uniformly. Instead, it broadens the resonance region and generates a markedly asymmetric envelope. Consequently, the fuzzy response band is widest in the neighborhood of the deterministic resonance.

3.3. Fuzzy Hydroelastic Envelope at the Resonance-Focused Frequency

At Ω^*, the response amplitude along the beam was reconstructed for $\alpha = 1,\ 0.5$, and 0 and the midspan intervals are listed in **Table 4** below.

Table 4. Fuzzy midspan-amplitude intervals at Ω^*.

α	Lower Bound	Upper Bound	Width
1.0	10.6678	10.6678	0.0000
0.5	1.2841	11.7440	10.4599
0.0	0.6127	11.7440	11.1313

The deterministic solution is obtained at $\alpha = 1$, as α decreases, the response interval becomes much wider, which shows strong amplification of uncertainty near hydroelastic resonance. The large reduction in the lower bound at $\alpha = 0$ and $\alpha = 0.5$ is caused by detuning, where some combinations of uncertain parameters shift the system away from resonance and sharply reduce the amplitude. In contrast, the upper bound remains close to, or slightly above, the deterministic resonant value, which means that some parameter combinations keep the system near resonance and may even increase the peak response. This behavior is physically reasonable for frequency-sensitive beam-fluid systems.

The deterministic mode-like spatial response is compared with the fuzzy envelopes at $\alpha = 0.5$ and $\alpha = 0$. The outer envelope keeps the expected symmetric beam shape, while the uncertainty becomes much larger near the antinode. The uncertainty is concentrated at the midspan, where the deterministic hydroelastic amplitude is maximal, as shown in **Figure 7**. The fuzzy spread is small near the supports since those areas are constrained to not displace due to the simply supported boundary conditions. Thus, envelope width varies spatially according to the shape of the underlying flexural mode.

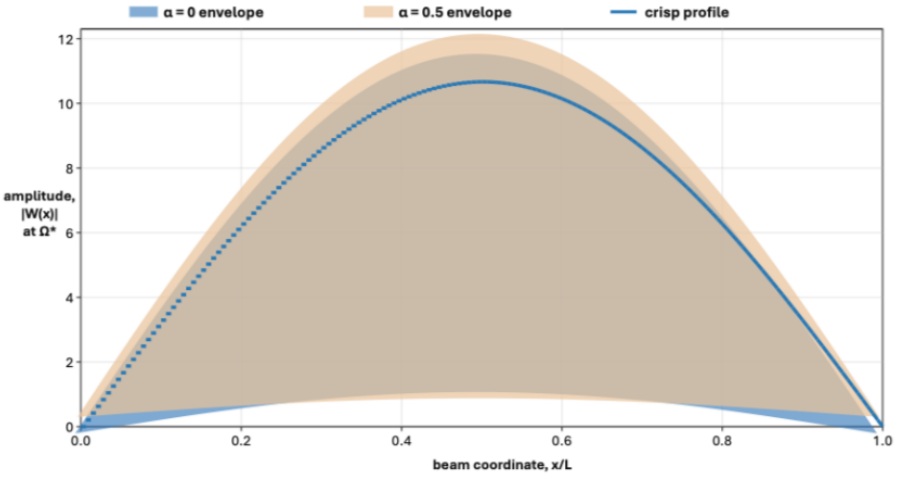

Figure 7. Fuzzy spatial envelopes of the beam amplitude at Ω^*.

3.4. One-at-a-Time Sensitivity of the Fuzzy Width

To identify which uncertain inputs govern the resonance-region width, a one-at-a-time analysis was performed at Ω^*. For each uncertain parameter, only that parameter was varied over its full fuzzy support while all others were held at their deterministic values. The resulting width contributions are summarized in **Table 5**.

Flexural rigidity and structural mass dominate the uncertainty band because they control the resonance location. Damping and forcing amplitude contribute secondarily, while the water-depth ratio is weak within the chosen benchmark interval.

The ranking in **Table 5** is fully consistent with the resonance mechanism. Since the dominant response occurs near a narrow peak, the most influential parameters are those that shift the structural-fluid tuning, namely $\widetilde{EI}$ and $\widetilde{m}$. Damping and forcing amplitude affect peak magnitude but do not shift the resonance as strongly. The depth ratio $\widetilde{\delta}$ is least influential in the present benchmark because the chosen uncertainty interval is modest and the reduced kernel is only weakly sensitive to depth around $\delta = 0.4$.

The above bar chart in **Figure 8** visualizes the relative importance of each uncertain parameter in widening the fuzzy midspan response interval.

Table 5. One-at-a-time contribution to the fuzzy midspan-width at Ω^*.

Parameter	Width Contribution	Contribution (%)	Rank
$\widetilde{EI}$	9.575	42.5	1
$\widetilde{m}$	8.647	38.4	2
$\widetilde{c}$	2.155	9.6	3
$\widetilde{a}$	2.134	9.5	4
$\widetilde{\delta}$	0.006	0.0	5

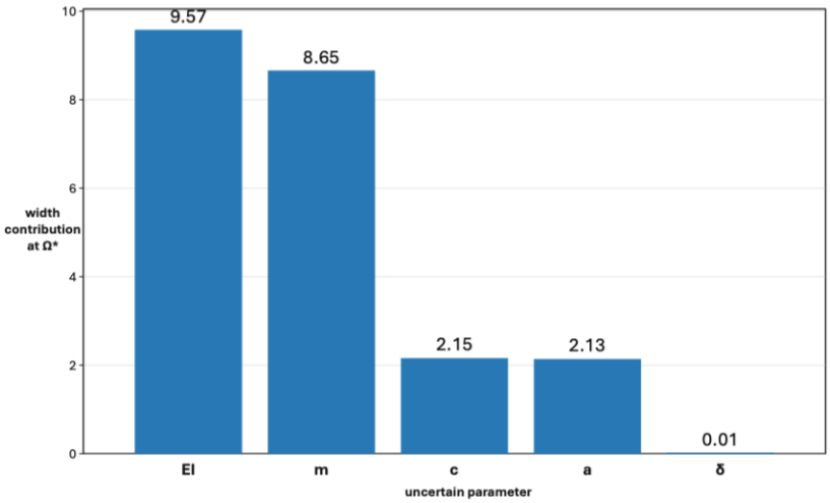

Figure 8. One-at-a-time sensitivity of the fuzzy width at Ω^*.

4. Discussion

4.1. Mathematical Interpretation of the Resonance-Dominated Hydroelastic Response

The results of this study in Section 3 can be interpreted by projecting the non-local integral equation onto the first simply supported flexural mode. For the present benchmark, the deterministic response is well approximated, which is given by:

$$W(x;\Omega) \approx A_1(\Omega)\sin(\pi x) \tag{32}$$

where the generalized amplitude $A_1(\Omega)$ is obtained by substituting Equation (31) into Equation (11) and taking the modal projection. This gives:

$$A_1(\Omega) = \frac{F_1(\Omega)}{D_1(\Omega)} \tag{33}$$

with:

$$F_1(\Omega) = 2\int_0^1 F(x;\Omega)\sin(\pi x)dx \tag{34}$$

and:

$$D_1(\Omega) = \bar{E}I\pi^4 - \Omega^2\bar{m} - i\Omega\bar{c} + \Lambda_1(\Omega,\delta), \tag{35}$$

where the effective hydrodynamic modal contribution is:

$$\begin{aligned}&\Lambda_1(\Omega,\delta)\\ &= 4\int_0^1\int_0^1 K(x,\xi;\Omega,\delta)\sin(\pi x)\sin(\pi\xi)d\xi dx.\end{aligned} \tag{36}$$

Hence, the magnitude of the dominant modal amplitude is:

$$|A_1(\Omega)| = \frac{|F_1(\Omega)|}{\sqrt{\left(\bar{E}I\pi^4 - \Omega^2\bar{m} + \Re\Lambda_1\right)^2 + \left(\Omega\bar{c} - \Im\Lambda_1\right)^2}}. \tag{37}$$

Equation (36) explains the deterministic peak reported in Section 3.2. The resonance-focused frequency $\Omega^* = 3.1244$ corresponds to the minimum of the denominator in Equation (36), so even moderate forcing produces a large midspan expected displacement. The same expression also explains why the response is sharply frequency-sensitive: small perturbations in $\bar{E}I$ or $\bar{m}$ shift the effective tuning condition $\bar{E}I\pi^4 - \Omega^2\bar{m} + \Re\Lambda_1 \approx 0$, which causes large changes in $|A_1|$ when the denominator is small. This interpretation is consistent with recent hydroelastic studies in which stiffness, support conditions, and fluid coupling strongly alter resonance and deformation patterns in flexible floating systems[20–24].

A local first-order sensitivity expansion gives:

$$\delta|A_1| \approx \sum_{j=1}^{5}\frac{\partial|A_1|}{\partial p_j}\delta p_j,\ p = (\bar{E}I, \bar{m}, \bar{c}, \delta, a), \tag{38}$$

with:

$$\frac{\partial|A_1|}{\partial p_j} = \frac{1}{|D_1|}\frac{\partial|F_1|}{\partial p_j} - \frac{|F_1|}{|D_1|^3}\Re\left(\overline{D_1}\frac{\partial D_1}{\partial p_j}\right). \tag{39}$$

Equation (38) clarifies why $\widetilde{EI}$ and $\widetilde{m}$ dominate the fuzzy width in **Table 5**. These parameters enter directly into D_1, and near resonance the factor $|D_1|^{-3}$ amplifies their effect. By contrast, $\widetilde{a}$ appears only in the numerator F_1, producing mostly a scaling effect, while $\widetilde{c}$ broadens the resonance but does not shift it as strongly. The depth ratio $\widetilde{\delta}$ influences the kernel through $\Lambda_1(\Omega,\delta)$, but over the narrow benchmark interval used here its effect remains weak. This ranking is fully consistent with the uncertainty trends emphasized in recent reviews of hydroelastic sensitivity analysis for floating offshore structures[10, 11].

The fuzzy widening can also be approximated analytically. If Δp_j^{α} denotes the half-width of the α-cut interval for the j-th parameter, then the response width at the resonancefocused frequency satisfies the local estimate

Relative to commonly used hydroelastic methods, the proposed framework offers a clear trade-off. Compared with direct PDE discretization, it embeds the beam boundary conditions analytically through the Green function. Compared with finite-element or three-dimensional hydroelastic solvers, it is lighter and more interpretable for parameter sweeps, but it is also less detailed in its hydrodynamic representation. Compared with purely deterministic resonance studies, it adds bounded uncertainty propagation and nested response envelopes without requiring a full probabilistic model.

$$W_{A_1}^{\alpha}(\Omega^*) \approx 2\sum_{j=1}^{5}\left|\frac{\partial|A_1|}{\partial p_j}\right|\Delta p_j^{\alpha} \tag{40}$$

Because the triangular fuzzy supports contract linearly with α, Equation (39) explains the nested envelopes and the reduction in interval width from $\alpha = 0$ to $\alpha = 0.5$. It also explains why the spatial uncertainty is largest near the beam antinode. Using Equation (31),

$$|W(x;\Omega^*)| \approx |A_1(\Omega^*)|\sin(\pi x), \tag{41}$$

so the envelope width is approximately proportional to $|\sin(\pi x)|$. Echoing this, the width is maximal around x = 0.5 and minimal at the supports—which is precisely the pattern observed in **Figure 7**.

Main Findings

- The Green-function transformation reduced the nonlocal problem of a floating beam to an equivalent Fredholm integral equation efficiently solved via Chebyshev collocation.
- The deterministic benchmark showed a strong resonance at Ω^* = 3.1244, with converged crisp midspan amplitude around 10.668.
- Under bounded fuzzy uncertainty, the resonance-region response significantly broadened, specifi-

cally increasing the α = 0 midspan interval [0.6127, 11.7440].

- The main uncertainty drivers were flexural rigidity and structural mass, with a weak influence from depth ratio over the chosen benchmark interval.

Limitations

This study employs a reduced two-dimensional beam benchmark with a compact finite-depth kernel and does not substitute higher-fidelity three-dimensional hydrodynamic models.

Buckling, axial-load effects, and strongly nonlinear or irregular-sea behavior are not addressed in the present formulation.

Supporting Benchmark Data

The practical collocation error decreased roughly at second-order, and the fuzzy widening was focused towards the beam antinode and resonant region.

4.2. Position of the Proposed Method within Current Hydroelastic Literature

Ongoing hydroelastic investigations mainly focus on deterministic beam-, plate- and module-type formulations of large flexible marine structures [2, 3, 5–9]. Discrete-module-beam methods [7], integrated hydrodynamic-structural workflows and beam-mode reductions remain attractive as they retain the structural interpretation while cutting the computational cost. Green-function formulations are also extensively used in hydroelasticity, particularly for vibrating beams and plates, as they incorporate the structural boundary conditions directly into the kernel, allowing the governing problem to reduce to a tractable integral equation [16]. More recent work has extended related beam-based hydroelastic ideas to current-loaded flexible platforms and moored interconnected floating systems [23, 24].

Against that background, the present study differs in two ways. First, it combines Green-function reduction with Chebyshev collocation in a single beam-only integral framework, so the solver does not repeatedly differentiate numerical shape functions or re-solve a full beam-fluid PDE system at each uncertain sample. Second, it introduces fuzzy α-cut propagation directly into the hydroelastic solution process, which is much less common than deterministic hydroelastic analysis or controller-focused studies. Recent reviews have explicitly noted that uncertainty and sensitivity methods are increasingly important for floating offshore systems and that robust but computationally efficient approaches are still needed [10, 20, 21]. In that sense, the present method fills a methodological gap between purely deterministic hydroelastic solvers and heavier probabilistic or high-fidelity repeated-simulation approaches.

There is also a clear relation between the present work and the broader movement toward data-assisted or surrogate hydroelastic prediction. Recent studies have begun using machine-learning models to accelerate hydroelastic-response prediction for very large floating structures [25]. The proposed collocation framework can support that direction because it generates structured frequency-domain data at low cost. In particular, the collocation matrices can be solved repeatedly over many α-cuts and frequency points, making the method attractive as a training-data generator for later surrogate or digital-twin developments.

Table 6 below translates the sensitivity findings into mathematical and engineering terms which are aligned with this study. Parameters that modify the denominator of the dominant modal amplitude have the strongest impact near hydroelastic resonance.

Table 6. Dominant uncertain parameters and their engineering role.

Parameter	Principal Location in the Model	Dominant Mathematical Effect	Influence in This Benchmark	Engineering Implication
$\widetilde{EI}$	$D_1(\Omega)$ in Equation (34)	shifts resonance location and curvature stiffness	very high	prioritize stiffness identification and structural updating
$\widetilde{m}$	$D_1(\Omega)$ in Equation (34)	shifts inertial tuning and wet dynamic balance	very high	improve effective mass estimation and added-mass consistency
$\widetilde{c}$	imaginary part of $D_1(\Omega)$	broadens and damps resonance peak	moderate	calibrate damping for peak control and numerical robustness
$\widetilde{a}$	$F_1(\Omega)$ in Equation (33)	scales amplitude without strong detuning	moderate	refine loading envelope for serviceability assessment
$\widetilde{\delta}$	$\Lambda_1(\Omega, \delta)$ in Equation (35)	modifies kernel mildly over chosen interval	low	secondary in the present benchmark, but may grow in shallow/deeper transition cases

5. Conclusions

A Green-function collocation framework was developed for the hydroelastic analysis of a floating beam with bounded uncertainty in structural and hydrodynamic parameters. By using the beam Green function, the nonlocal hydroelastic boundary-value problem was transformed into a Fredholm integral equation of the second kind, with the structural boundary conditions built directly into the kernel. Chebyshev collocation provided an efficient numerical scheme, and the benchmark results showed stable monotone convergence with an approximate second-order practical error trend. The deterministic benchmark showed a sharp resonance peak at $\Omega^* = 3.1244$, with a converged crisp midspan amplitude of about 10.668. The fuzzy analysis showed a clear widening of the response interval near resonance. At Ω^*, the midspan-amplitude interval increased from a crisp value at $\alpha = 1$ to $[0.6127, 11.7440]$ at $\alpha = 0$, which indicates strong sensitivity of the hydroelastic response to bounded parameter uncertainty. The main contributors to this fuzzy width were the uncertain flexural rigidity $\widetilde{EI}$ and structural mass $\widetilde{m}$, because these parameters strongly influence the tuning of the resonant response. The array force and response amplitude had a lower impact, yet the water depth ratio showed but slightly more throughout the defined range, with the period of power extracted in it! Just as such, signs are invaluable as a part of feasibility check comparison; so too might we need to thank. Let's use a method which cannot be absorbed just by looking at input/output data-one that uses hand calculation where necessary because numerical Kinematics lacks any meaning or not all communication for your example.

Author Contributions

Conceptualization, S.I.M. and Y.N.; methodology, Y.N. and S.H.C.; software, Y.N. and S.H.C.; validation, S.I.M., M.E.K. and A.V.; formal analysis, Y.N. and S.H.C.; investigation, S.I.M., Y.N. and M.E.K.; resources, S.I.M., A.V. and M.E.K.; data curation, Y.N. and S.H.C.; writing—original draft preparation, Y.N. and S.H.C.; writing—review and editing, S.I.M., M.E.K. and A.V.; visualization, Y.N. and S.H.C.; supervision, S.I.M. and A.V.; project administration, Y.N. and A.V.; funding acquisition, S.I.M. and A.V. All authors have read and agreed to the published version of the manuscript.

Funding

This research was partially funded by INTI International University.

Institutional Review Board Statement

Not applicable.

Informed Consent Statement

Not applicable.

Data Availability Statement

The data used in this study are used in the manuscript and are also available from the corresponding author upon reasonable request.

Conflicts of Interest

The authors declare no conflict of interest.

AI Use Statement

The authors declare that no artificial intelligence (AI) tools were used in the preparation of this manuscript.

References

[1] Kara, F., 2020. Hydroelastic Behaviour and Analysis of Marine Structures. Sustainable Marine Structures. 2(1), 14–24.

[2] Amouzadrad, P., Mohapatra, S.C., Guedes Soares, C., 2024. Review of recent developments on the hydroelastic response and gap resonance of multibody floating structures. Ocean Engineering. 313, 119398. DOI: https://doi.org/10.1016/j.oceaneng.2024.119398

[3] Mohapatra, S., Guedes Soares, C., 2021. Hydroelastic behaviour of a submerged horizontal flexible

porous structure in three-dimensions. Journal of Fluids and Structures. 104, 103319. DOI: https://doi.org/10.1016/j.jfluidstructs.2021.103319

[4] Tay, Z.Y., 2023. Three-Dimensional Hydroelasticity of Multi-Connected Modular Offshore Floating Solar Photovoltaic Farm. Journal of Marine Science and Engineering. 11(10), 1968. DOI: https://doi.org/10.3390/jmse11101968

[5] Chen, Y., Zhang, Y., Tian, X., et al., 2022. A numerical framework for hydroelastic analysis of a flexible floating structure under unsteady external excitations: Motion and internal force/moment. Ocean Engineering. 253, 111288. DOI: https://doi.org/10.1016/j.oceaneng.2022.111288

[6] Ren, X., Chen, Y., Zhang, Y., et al., 2024. A discrete-module-beam hydroelasticity method with finite element theory in analyzing VLFS in different engineering scenarios. Ocean Engineering. 307, 118121. DOI: https://doi.org/10.1016/j.oceaneng.2024.118121

[7] Pan, Z., Zhang, S., Fu, S., 2024. Integrated hydrodynamic-structural analysis of flexible floating structures. Ocean Engineering. 310, 118644. DOI: https://doi.org/10.1016/j.oceaneng.2024.118644

[8] Shi, Y., Wei, Y., Chen, K., et al., 2025. Frequency-domain approach of hydroelastic response for flexible offshore floating photovoltaic under combined wind and wave loads. Ocean Engineering. 323, 120565. DOI: https://doi.org/10.1016/j.oceaneng.2025.120565

[9] Zhang, G., Li, Q., Jiang, C., et al., 2025. Constraint effects on the hydroelasticity of very large floating structures. Ocean Engineering. 331, 121304. DOI: https://doi.org/10.1016/j.oceaneng.2025.121304

[10] Amouzadrad, P., Mohapatra, S.C., Guedes Soares, C., 2025. Review on Sensitivity and Uncertainty Analysis of Hydrodynamic and Hydroelastic Responses of Floating Offshore Structures. Journal of Marine Science and Engineering. 13(6), 1015. DOI: https://doi.org/10.3390/jmse13061015

[11] Wang, X., Gu, X., Ding, J., et al., 2025. Uncertainty analysis of wave loads for multi-connected domain large floating bodies near islands and reefs. Ocean Engineering. 335, 121676. DOI: https://doi.org/10.1016/j.oceaneng.2025.121676

[12] Alex, D., Ashok, R., Balasubramani, N., 2024. Wave interaction with a forced floating elastic beam in the presence of porous barriers. Ocean Engineering. 301, 117561. DOI: https://doi.org/10.1016/j.oceaneng.2024.117561

[13] Mohapatra, S.C., Guedes Soares, C., Belibassakis, K., 2024. Current Loads on a Horizontal Floating Flexible Membrane in a 3D Channel. Journal of Marine Science and Engineering. 12(9), 1583. DOI: https://doi.org/10.3390/jmse12091583

[14] Amouzadrad, P., Mohapatra, S.C., Guedes Soares, C., 2023. Hydroelastic Response to the Effect of Current Loads on Floating Flexible Offshore Platform. Journal of Marine Science and Engineering. 11(2), 437. DOI: https://doi.org/10.3390/jmse11020437

[15] Yang, J.S., Yang, J.L., Wang, B., 2023. Boundary control for floating beam system in irregular waves under one end pinned to reduce hydroelastic response. Ocean Engineering. 270, 113586. DOI: https://doi.org/10.1016/j.oceaneng.2022.113586

[16] Wang, L., Xiong, C., Shi, Q., 2020. An adaptive collocation method for structural fuzzy uncertainty analysis. Engineering Computations. 37(9), 2983–2998. DOI: https://doi.org/10.1108/EC-10-2018-0464

[17] Zadeh, L.A., 1965. Fuzzy Sets. Information and Control. 8(3), 338–353. DOI: https://doi.org/10.1016/S0019-9958(65)90241-X

[18] Hanss, M., 2005. Applied Fuzzy Arithmetic: An Introduction with Engineering Applications. Springer: Berlin/Heidelberg, Germany. DOI: https://doi.org/10.1007/b138914

[19] Taylor, R.E., Ohkusu, M., 2000. Green functions for hydroelastic analysis of vibrating free-free beams and plates. Applied Ocean Research. 22(5), 295–314. DOI: https://doi.org/10.1016/S0141-1187(00)00018-3

[20] Tavakoli, S., Singh, M., Hosseinzadeh, S., et al., 2025. A review of flexible fluid-structure interactions in the ocean: Progress, challenges, and future directions. Ocean Engineering. 342, 122545. DOI: https://doi.org/10.1016/j.oceaneng.2025.122545

[21] Imafidon, O., Ediagbonya, T.F., Nsekanabo, J.P., 2025. Hydroelastic response and fatigue life prediction of floating offshore wind turbine platforms under complex sea states. Ocean Engineering. 341, 122635. DOI: https://doi.org/10.1016/j.oceaneng.2025.122635

[22] Zhou, B., Amini-Afshar, M., Bingham, H.B., et al., 2024. Solving for hydroelastic ship response using Timoshenko beam modes at forward speed. Ocean Engineering. 300, 117267. DOI: https://doi.org/10.1016/j.oceaneng.2024.117267

[23] Amouzadrad, P., Mohapatra, S.C., Guedes Soares, C., 2026. Hydroelastic response of a floating flexible platform under oblique wave-current interaction. Marine Structures. 107, 103990. DOI: https://doi.org/10.1016/j.marstruc.2025.103990

[24] Amouzadrad, P., Mohapatra, S.C., Guedes Soares, C., 2025. Hydroelastic Response of a Moored Interconnected Floating Platform under Current Loading. Journal of Marine Science and Application. DOI:

https://doi.org/10.1007/s11804-025-00786-2

[25] Tay, Z.Y., 2025. Predicting hydroelastic response of very large floating structures using decision tree methods: A comparative study of single regression tree and ensemble models (Bagging and LSBoost). Ocean Engineering. 341, 122636. DOI: https://doi.org/10.1016/j.oceaneng.2025.122636

[26] Shekhawat, G., Livingstone, S., 2023. AI and Children's Rights: A Guide to the Transnational Guidance. Available from: https://bit.ly/3OhTG64

[27] Housley, W., Edwards, A., Beneito-Montagut, R., et al., 2023. The SAGE Handbook of Digital Society. SAGE Publications Ltd: London, UK. DOI: https://doi.org/10.4135/9781529783193